INTER-NOISE 2021 Congress
(1–4 August 2021, Online and in Washington DC, USA)

Design of axial flow fans for reduced noise and improved efficiency

Erika Quaranta[1] and Malcolm Smith[2]

ISVR Consulting,

University of Southampton, UK

ABSTRACT

Axial flow fans are used in a wide variety of applications, from cooling systems for electronics to ventilation in buildings. Whatever the application, there will be competing design constraints which make it difficult to achieve the required pressure-flow performance characteristic, within a specified space envelope, whilst meeting a target aerodynamic efficiency and noise level.

This paper describes a design methodology for optimizing aerodynamic performance and noise. It uses a semi-analytic 2-D design tool for preliminary predictions, combined with a 3-D numerical CFD analysis to visualize the flow and validate assumptions. Both models can be extended to the design of multi-stage systems.

The 2-D model predicts the flow velocity at the trailing edge of the blades for each point on the fan performance curve, which is then used to estimate self-noise characteristics of the rotor using a classical model of aerofoil trailing edge noise. The CFD analysis provides detailed validation of assumed aerofoil characteristics, including the effect of 3D design features such as blade sweep, and confirms the flow and aerodynamic efficiency predictions; it can also be used to estimate parameters such as turbulence intensity that is a key driver for the noise level of the rotor and stators.

1. INTRODUCTION

Axial flow fans used for cooling electronics equipment need to provide good aerodynamic performance in a tight space envelope. The design methodology reported here was developed during a study to increase efficiency and reduce noise of the two stage axial flow fan shown in Figure 1a, whilst still providing the pressure and flow requirements of the system within the size constraint.

There are many textbooks and research papers about aerodynamic performance of axial flow fans which discuss noise issues in general terms [e.g. 2, 3, 4], and many other publications which consider noise but are more limited with respect to performance. The aim here is to develop a unified approach to both aspects.

An issue for any engineering design tool is the complexity of the prediction methods: numerical models can be accurate but are difficult and computationally expensive to use, and do not readily indicate how a design can be improved; analytical models are likely to be less accurate, but can provide rapid results for initial optimization. Here again we aim to provide a unified approach by linking

[1] E.Quaranta@soton.ac.uk

[2] mgs@isvr.soton.ac.uk

the best attributes of a 2D analytic model and a 3D numerical model, as discussed in Sections 3 and 4 respectively.

2. MEASUREMENTS OF PERFORMANCE AND NOISE FOR THE BASELINE FAN

The aerodynamic performance of axial flow fans is assessed using a standard test rig in which the volume flow Q is measured as pressure change across the fan ΔP is varied, producing a P-Q working line for a particular fan speed [1]. Aerodynamic tests on the fan had been carried out previously using such a rig, but for the purposes of this study the simplified rig shown in Figure 1b was built. This had adaptations to reduce rig noise so that aerodynamic performance and noise could be measured simultaneously. Besides the pitot tube, which was calibrated to measure volume flow, electrical power to the fan was also monitored. Measurements in the standard rig were made at full speed of 15000 RPM, whereas in the noise rig the normal 9000 RPM operating speed was used. Data may be scaled using the fan laws, taking account of motor efficiency at each speed.

Measurements were taken for single and two-stage configurations of the fan, with and without the honeycomb insert. Although the noise rig is greatly simplified compared with a standard rig, flow and efficiency data agreed well with the standard data. The highest flow rates could not be achieved in the noise rig because there was no system to compensate for flow losses [1].

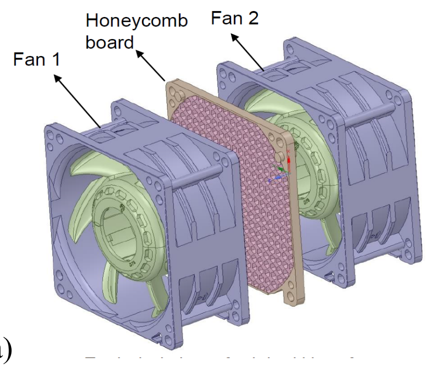

a)

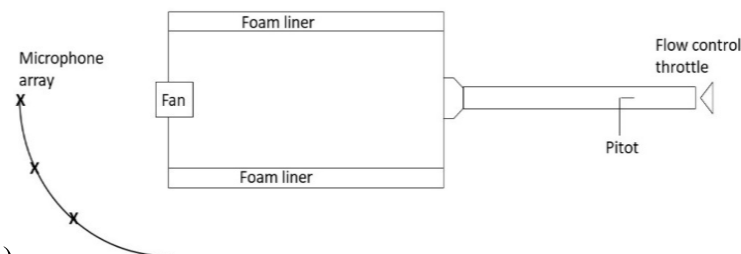

b)

Figure 1: a) Baseline two-stage fan design. b) Test rig for combined noise and flow measurements.

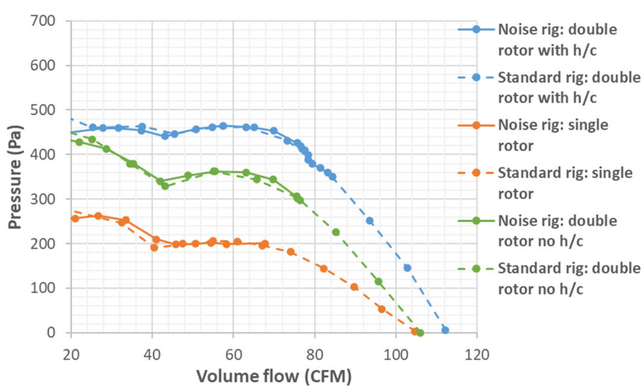

a)

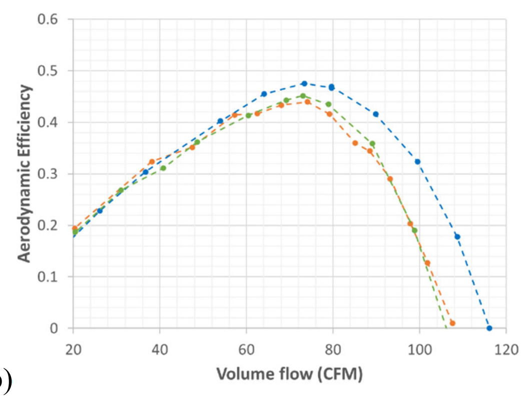

b)

Figure 2: Aerodynamic performance of the single and two-stage baseline fan, with and without honeycomb, at 9000 RPM. a) P-Q data; b) aerodynamic efficiency (standard rig data only for clarity).

Peak pressure occurs at a flow rate of approximately 70 CFM, which is close to the normal working point of the system. As the flow restriction is increased the fan starts to stall and both flow rate and working pressure are reduced. The prediction methods outlined below are for fans prior to stall, and so do not predict the pressure rise below 40 CFM where the rotor is fully stalled. The data show that the honeycomb significantly improves the performance of the two-stage fan by removing swirl from stage 1 to ensure that flow into rotor 2 is axial.

Noise data were analyzed into 1/3 octave and narrow band spectra, Figure 3b, and averaged over all microphones to give a mean far-field sound pressure level (SPL). From the rotational speed and blade numbers of the fan, the narrow band spectrum may be used to distinguish between tonal noise and broadband noise. Even at constant speed this analysis must take account of the effect of the analysis system in broadening the peaks, and so a summation of energy around each harmonic of blade passing frequency (BPF) is carried out, i.e. the spectral points marked red in Figure 3a. The remainder of the spectrum is taken as the broadband noise.

Applying the A-weighting function to the narrow band spectrum, the contribution of tonal and broadband noise to the overall A-weighted level may be plotted as a function of volume flow rate, Figure 3b, from which it may be seen that broadband noise is dominant for this fan. Broadband noise is about 3dB higher for the double rotor compared with the single rotor, but the increase in tonal noise is closer to 5dB because of the higher inflow turbulence to rotor 2. Tonal noise is relatively low because of the strong sweep of the stators, as shown in Figure 7c, and it was confirmed experimentally that the main source of broadband noise was likely to be the trailing edge of the rotor.

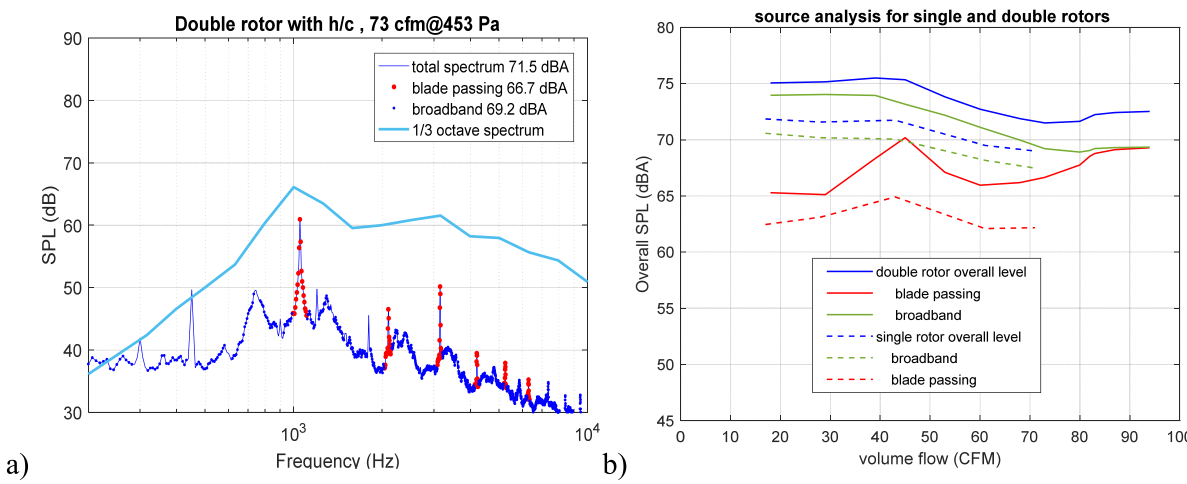

Figure 3: a) Double rotor noise data for 73 CFM @453 Pa at 9000 RPM. b) Source breakdown between broadband and blade passing frequency noise for the single and double rotors.

3. ANALYTIC PREDICTION MODEL FOR FAN PERFORMANCE AND NOISE

3.1. Calculation of P-Q characteristic

The fan design method described here broadly follows that set out by Bleier [2], which assumes a uniform inflow and aims to achieve the same pressure rise at all radial locations, i.e. the free-vortex flow used by Wallis [3]. Since the aim here is to build a comprehensive model of both aerodynamic performance and efficiency, we also draw on theory set out in the reference book by Eck [4].

Fan design involves the selection of design parameters, illustrated in Figure 4a, such as the number or spacing of blades, and the blade profile, chord and angle for each radial location. Three radial locations are considered here, at 1/6, 1/2 and 5/6 of annulus height and labelled radius 1-3 respectively on graphs, and for each radius the local lift and drag forces on each blade are given by

$$L = C_l \frac{\rho V_1^2 l b}{2} \quad ; \quad D = C_d \frac{\rho V_1^2 l b}{2} \tag{1}$$

Here l is chord and b is span of the section of blade under consideration and ρ is air density. The lift and drag coefficients, C_l and C_d, are functions of angle of incidence α_{inc}. This varies with the intake flow relative to the moving blade, which has magnitude V_1 and angle β relative to the rotor plane. Estimating C_l and C_d requires use of an aerofoil analysis code such as Xfoil, [5], or reference tables such as Abbott, [6], bearing in mind that for small fans there may be a Reynolds number dependence. At the working point of this fan *Re* based on chord ranged from 3e4 to 7e4.

For both the baseline and modified rotor designs discussed here the values of lift and drag coefficient given in [2] for the NACA 6512 profile were used, reduced by a factor of 0.7 to account for Reynolds number. These are plotted in Figure 5. This was a significant assumption for the baseline rotor, although the results in Section 5 indicate that it was reasonable.

The flow onto the blade is calculated using the velocity diagram of Figure 4b. Because 2-stage fans are under consideration, this is a general diagram that accounts for non-axial inflow, with the inflow given by vector $\boldsymbol{c}_1$ at angle δ_1 to the axis. In the case shown here δ_1 and rotational component c_{1r} are negative, which represents counter-rotation relative to the motion of the rotor blade; for co-rotation c_{1r} and δ_1 will be positive, but in each case the mathematics below is the same.

By continuity the axial flow component V_0 is the same throughout the fan. The axial flow, blade velocity V_b and blade spacing t are related to the volume flow in m^3/s, Q, the duct area A, rotational speed in RPM, N, and number of blades Z_b, as follows:

$$V_0 = \frac{Q}{A}\ ; \quad V_b = \frac{2\pi RN}{60}\ ; \quad t = \frac{2\pi R}{Z_b} \tag{2}$$

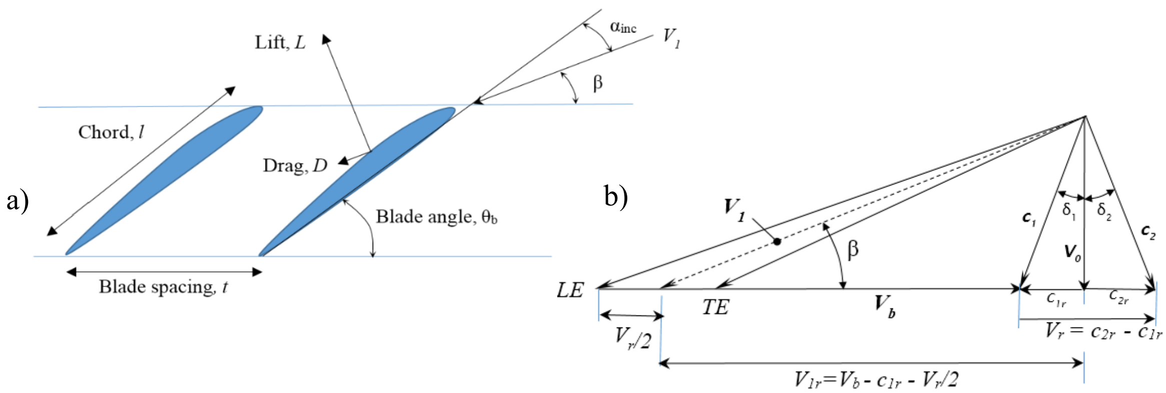

Figure 4: a) Dimensions, angles and force diagram for an airfoil in a cascade; b) General velocity triangle for a rotor with non-axial inflow.

The rotor adds momentum to the flow to give outlet flow vector $\boldsymbol{c}_2$. This change is represented by rotational velocity $V_r = c_{2r} - c_{1r}$, which is related to pressure rise for the rotor using the turbine equation:

$$V_r = \frac{\Delta P}{\rho V_b \eta_1} \tag{3}$$

Here η_1 is an empirical parameter that is implicit in the method of [2], where a value of 0.69 is used. A similar value of $\eta_1 = 0.7$ was found to work well in this model, though the physical purpose of this empirical parameter is still being investigated.

Noting that $V_{1r} = V_b - c_{1r} - \frac{V_r}{2}$, the magnitude and angle of the incident flow are given by Equation 4. The pressure rise due to lift ΔP and pressure loss due to drag $\Delta P'$ are then given by Equation 5, [4].

$$V_1 = \sqrt{V_{1r}^2 + V_0^2}\ ; \quad \beta = tan^{-1}\left(\frac{V_0}{V_{1r}}\right)\ ; \quad \alpha_{inc} = \theta_b - \beta \tag{4}$$

$$\Delta P = C_l \frac{l}{t} V_1 V_b \frac{\rho}{2}; \qquad \Delta P' = C_d \frac{V_1}{V_0}\frac{V_1^2}{2}\rho\frac{l}{t} \tag{5}$$

Because of the inter-dependence of V_r , V_1 and ΔP, an iterative solution of these equations is required. This is implemented in the model by specifying an initial value for ΔP as the nominal target pressure change, a value of V_r is calculated from Equation 3, then a new estimate for ΔP is obtained from Equation 5. To ensure stable convergence it was found necessary to slow the process down by specifying a reduced step size for ΔP.

Because of the pressure loss in the rotor given by Equation 5, the iteration uses the net pressure $\Delta P_{net} = \Delta P - \Delta P'$. Other flow losses are also taken into account via an empirical secondary drag coefficient. The magnitude and angle of the outlet flow, c_2 and δ_2 are also calculated for use in stator design.

Besides the assumed lift and drag characteristics, Figure 5a also shows the iterated angle of incidence and lift coefficient for each flow rate. The iterated solution for the P-Q curve at each radius is presented in Figure 5b, from which it is apparent that the tip of the blade, radius 3, is predicted to stall below a flow rate of 80 CFM because the angle of incidence is close to 20°.

The fact that the predicted pressure rise from the three blade sections are significantly different means that this baseline design does not provide a free-vortex flow, and will be prone to 3-D flow effects which will reduce efficiency and pressure. This result is dependent on the accuracy of the assumed values for C_l and C_d, which is discussed in Section 5, and the modified rotor described in Section 6 is designed to provide a better pressure balance, nonetheless the peak overall pressure of 200 Pa is in good agreement with the measured data in Figure 1a.

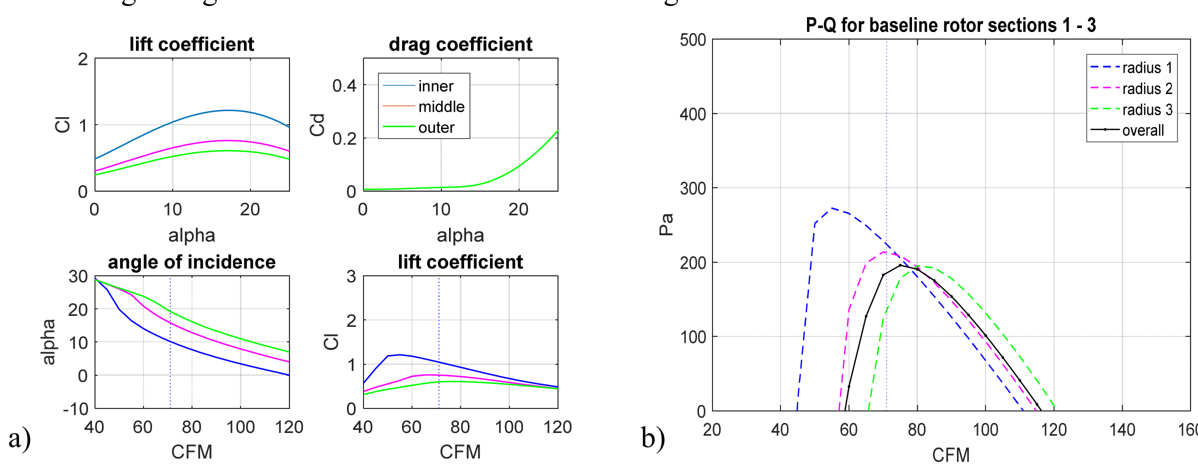

Figure 5: a) Assumed lift and drag as a function of α_{inc} and flow rate. b) Predicted P-Q for the single stage baseline rotor at 9000 RPM.

3.2. Calculation of rotor efficiency

Having determined the incident velocity components and lift and drag forces, the total rotational and axial force (thrust), F_{rot} and F_{ax}, applied to the Z_b blades at each radius are:

$$F_{rot} = Z_b(L\,sin(\beta) + D\,cos(\beta)) \;\; ; \;\; F_{ax} = Z_b(L\,cos(\beta) + D\,sin(\beta)) \tag{6}$$

The power input to j^{th} section of the rotor and total input power for the whole rotor are then:

$$W_{in,j} = F_{rot,j}V_{b,j} \;; \quad W_{in} = \sum_j W_{in,j} \tag{7}$$

The power output for each section of blade is calculated from the total pressure change multiplied by the volume flow rate through that section of rotor, and the total power output is again obtained by summing over all sections

$$W_{out,j} = \Delta P_{net,j}Q_j \;; \quad W_{out} = \sum_j W_{out,\,j} \tag{8}$$

From the power input and power output, the efficiency and an area weighted mean pressure are:

$$\eta_{tot} = \frac{W_{out}}{W_{in}} \quad ; \quad \overline{\Delta P_{net}} = \frac{W_{out}}{Q} \tag{9}$$

As noted above any significant pressure imbalance between different sections of blade will lead to 3-D flow effects which would invalidate the 2-D approach used here, and might reduce the overall delta pressure and fan efficiency.

Figure 6a shows the efficiency of the three blade sections, from which it is apparent that at the 70 CFM working point the tip of the blade is least efficient because it is so close to stall. The peak overall efficiency of 51% is higher than the measured value of 45% in Figure 2, which may be due to many causes: 3D flow, inaccurate lift data, inaccurate primary or secondary drag, etc.

The analytic model was also used to predict the performance of two-stage fans, with an appropriate boundary condition to account for the honeycomb. There is insufficient space to include predictions here, but they agreed well with Figure 2, and in particular the improved efficiency of the 2-stage rotor was attributed to the fact that the secondary drag is the same as for the single rotor case.

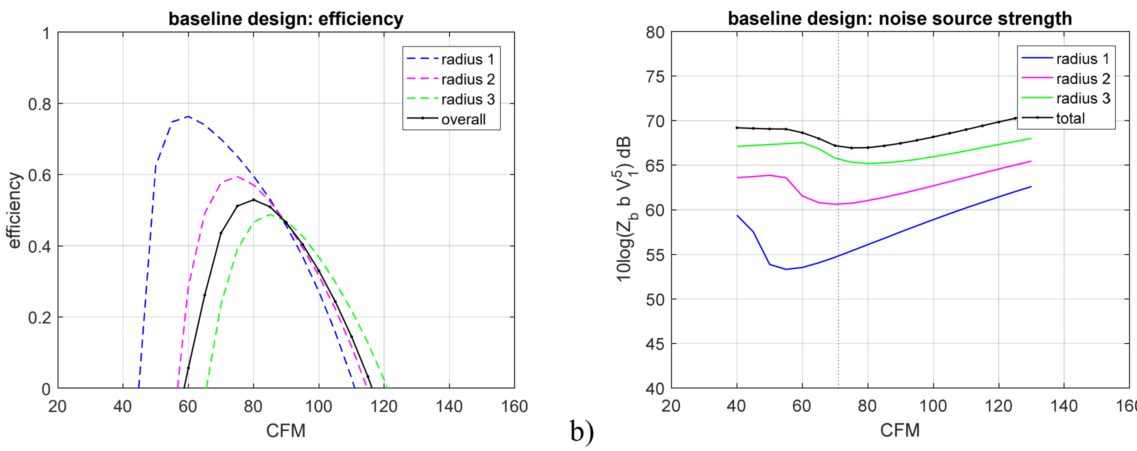

a)

Figure 6: Predictions for each radial location of the baseline rotor versus flow rate: a) Efficiency; b) Noise source strength.

3.3. Model of noise source strength

The flow data from the aerodynamic model may be used as the basis of a basic noise prediction model. For the trailing edge source described by Ffowcs-Williams and Hall [7], which was assessed by rig testing as probably the dominant source for this fan operating in a clean flow, the mean square acoustic pressure scales as:

$$< p^2 > \approx \rho^2 u_0^2 V_1^2 M_v \left(\frac{b l_3}{R^2}\right) F(\theta) \tag{10}$$

Here u_0^2 is turbulence intensity and M_v is convection Mach number for turbulence at the trailing edge, which combined with the V_1^2 term give a combined flow dependency of V_1^5. As before b is the blade span, and since there are Z_b blades the total source length for this section of rotor is $Z_b b$. Other terms in Equation 10 (spanwise correlation length l_3, observer distance R, and source directivity F(θ)) are neglected at this stage. Thus a simple noise source strength in decibels for each blade section can be approximated by:

$$L_p = 10\, log_{10}(Z_b b V_1^5) \tag{11}$$

Other sources, such as those due to inflow turbulence, blade tips and stators are not included at present. An overall source level for the complete rotor is obtained by a decibel sum of the three sections. The trailing edge noise source strength for the baseline rotor given in Figure 6b indicates that the overall noise will be dominated by the tip section of the blade, where the flow velocity is highest. The model suggests that trailing edge noise reduces in level as flow rate drops, although in the measured data of Figure 3b this is not seen because blade stall noise becomes dominant.

4. NUMERICAL MODEL OF FAN PERFORMANCE

The CAD geometry was used to generate a model suitable for CFD analysis. This captured the basic geometrical features of the rotor and stator blades, while simplifying and extending the external ducts to include the inlet and outlet. Figure 7 shows the entire fluid volume, including the inlet duct extended in length by twice the rotor duct diameter *D*, and the outlet chamber which is 3 times larger than the rotor duct and 3*D* in length. All ducts were modelled as axisymmetric to simplify the model. Various details of the surface mesh are also shown in Figure 7, and the total number of mesh elements was about 20M.

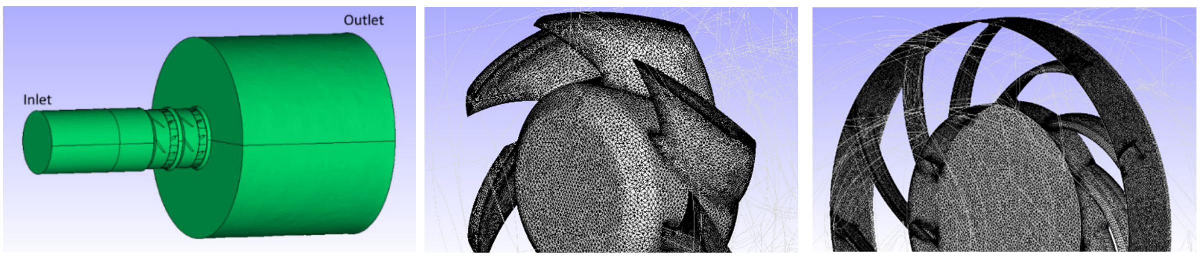

Figure 7: Total fluid volume of the CFD model, including the double rotor/stator, inlet duct and outlet chamber and details of the surface mesh.

The honeycomb board was difficult to model in detail, but it was clear from the tests that its effect was not negligible. Thus a simplified model of the board was developed, comprising zero thickness cells as circular sectors aimed at maintaining the area equal to the original honeycomb.

The CFD analysis was performed in Ansys Fluent using RANS and the k-ω SST turbulence model for incompressible flow. The outlet pressure was fixed at ambient, while the inlet total pressure was varied to run several points on the P-Q curve, using as monitors of convergence the volume flow rate at the inlet and outlet. The volume surrounding the rotors was rotating at a fixed rotational speed either as frame motion (steady state) or mesh motion (transient), with the former preferred because it is much cheaper computationally. Generally, points on the curve at low delta pressure / high flow rate converged well using steady analysis, while at higher pressure / lower flow rates, close to rotor stall, convergence was more difficult, and the transient approach was used.

4.1. Comparison of fan performance with experiments

Performance of three fan configurations are compared with test results: the double rotor/stator with and without honeycomb board, and a single rotor/stator model. The latter was especially useful for developing the rotor to improve performance as described in Section 6. All results were obtained for a rotor speed of 15000 RPM, since this was the speed for which motor efficiency was known.

Figure 8 compares the predictions and measurements for the pressure/volume flow rate and aerodynamic fan efficiency which was evaluated as

$$\frac{W_{out}}{W_{in}} = \frac{\Delta P\ Q}{T\omega} \tag{12}$$

Where T is torque and ω is rotational velocity in rad/s.

The overall trend for both P-Q and efficiency are respected, but CFD results are generally over-predicting the fan performance by about 10%. This is particularly evident for the configuration including the honeycomb, possibly because the idealized zero thickness geometry of the board does not include much loss.

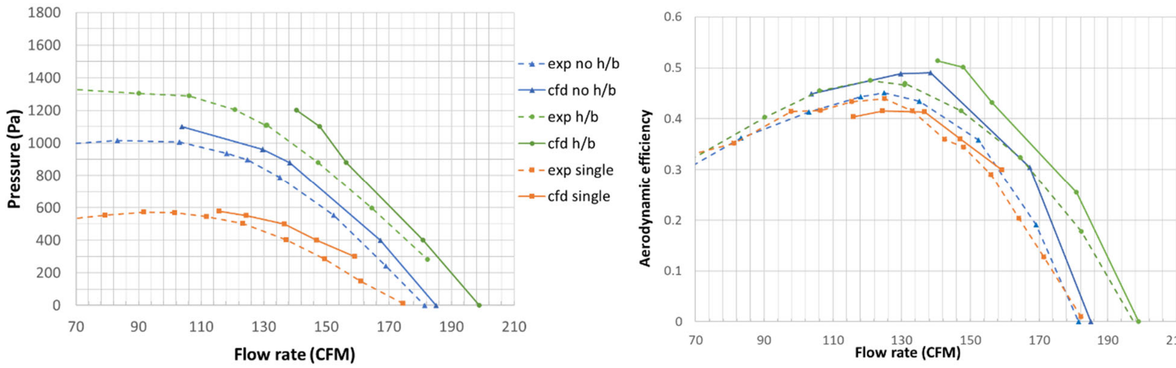

Figure 8: Comparison of CFD predictions with test data at 15000 RPM: a) P-Q curves for the three different fan configurations; b) aerodynamic efficiency.

5. CORRELATION OF THE 2D AND 3D MODELS

Using the integration tools in Fluent, the CFD results were used to calculate the axial and rotational forces, F_{ax} and F_{rot} , for five radial blade sections, and also the mean axial and rotational flow components. From these data it is possible to infer the lift and drag coefficients that would need to be used in the analytic prediction model to obtain the same result. This is based on reverse use of the theory outlined in Section 2. Ideally the process would take into account the pressure loss due to secondary drag mentioned previously, though this has not yet been included.

The single rotor CFD model provides a calculated volume flow Q for a number of specified pressure boundary conditions ΔP. The volume flow may be used in Equation 2 to calculate the mean axial flow velocity into the rotor, although A is about 15% smaller than the true duct area because of the duct boundary layer and tip feature of the rotor.

Equation 3 is then used to calculate the rotational flow component V_r, using $\eta_1 = 0.7$ as before, and from the blade velocity V_b the incident flow velocity V_1 and angle β are calculated from Equation 4. The simultaneous Equations 6 may then be solved for L and D:

$$L = \frac{F_{rot}}{Z_b} sin(\beta) + \frac{F_{ax}}{Z_b} cos(\beta)\,; \quad D = \frac{F_{rot}}{Z_b} cos(\beta) - \frac{F_{ax}}{Z_b} sin(\beta) \tag{13}$$

From these estimates of the lift and drag forces, together with the incident flow velocity V_1, the lift and drag coefficients may be obtained from Equations 1.

Using the 500 Pa data as an example, Figure 9 shows the derived velocity and force data at this pressure condition for each radial location, and the resultant flow angles and effective coefficient of lift. A value of $\eta_1 = 0.7$ has been used here, as in the analytic model.

Going through the same process for other pressures gives coefficient of lift-vs-angle of incidence values for 5 pressure points and 5 radial locations. These are plotted in Figure 10, and the C_l data used in the analytic model are also shown for comparison. Some interpolation for radial position is required to compare the two data sets, but it is apparent that there is reasonable agreement between the CFD data and the values assumed in the analytic model, especially at the higher angles of incidence where the fan would normally operate. The clear trend of higher C_l at the root and lower C_l at the tip is also in good agreement.

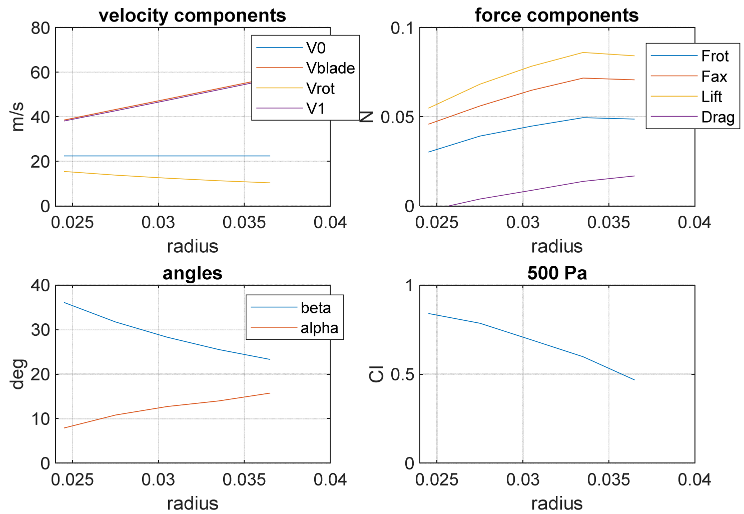

Figure 9: Derived flow, force, angles and C_l data for baseline design at 500Pa.

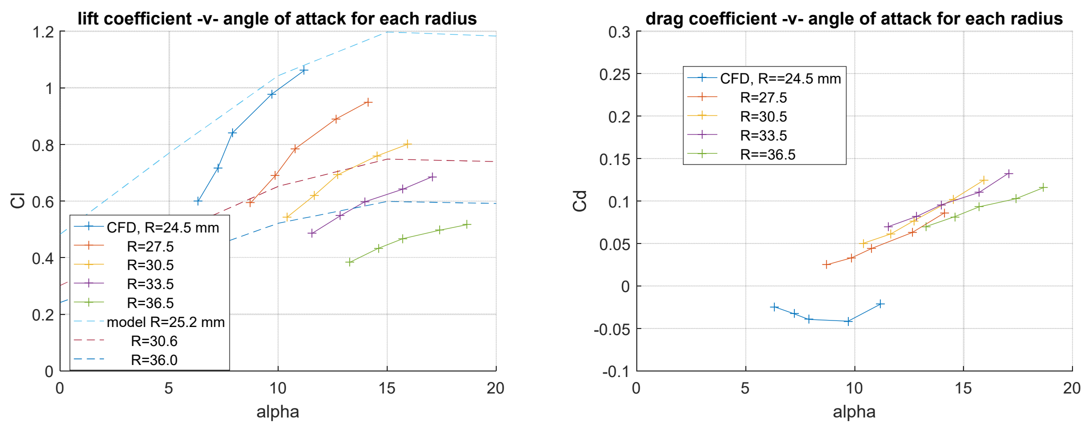

Figure 10: Inferred aerodynamic lift and drag coefficients for the baseline single rotor.

Data for the drag coefficient may also be extracted, though this is less accurate as Equation 6 indicates that this comes from the difference of two relatively large forces. Nonetheless the calculated drag coefficients of 0.05-0.1 are in reasonably good agreement with values assumed in the analytic model, except at the root where a negative value is obtained probably because of 3D flow effects.

6. METHODOLOGY FOR IMPROVING THE DESIGN

Both the prediction models indicate that at the normal working point of the baseline fan the outer portion of the blade is working at high angles of incidence, so that the ratio of lift/drag is relatively low, and also there is a pressure imbalance between the blade sections. The strategy used to improve the design was to reduce angle of incidence at the tip to improve efficiency and better balance the blade pressure profile, and to increase chord and/or lift coefficient to improve the pressure ratio at the required flow rate. With a more efficient rotor providing an increased pressure at the required flow rate, it should then be possible to reduce noise by running the rotor at lower speed.

6.1. Analytic model

The modified blade was based on the NACA 6512 profiles suggested in [2], and Figure 11 shows a comparison of the original and modified profiles, blade angles and chords. Figure 12 then shows the P-Q working line and blade pressure distribution predicted by the 2-D model, indicating that the modifications are predicted to produce a well-balanced rotor that better fulfils the aim of a free-vortex flow. Pressure and efficiency at the 70 CFM working point is significantly improved. Although there is almost no change in noise level, the improved pressure of 250 Pa means that a speed reduction from 9000 to 8300 RPM should be possible, which would give 2.5 dB reduction in noise.

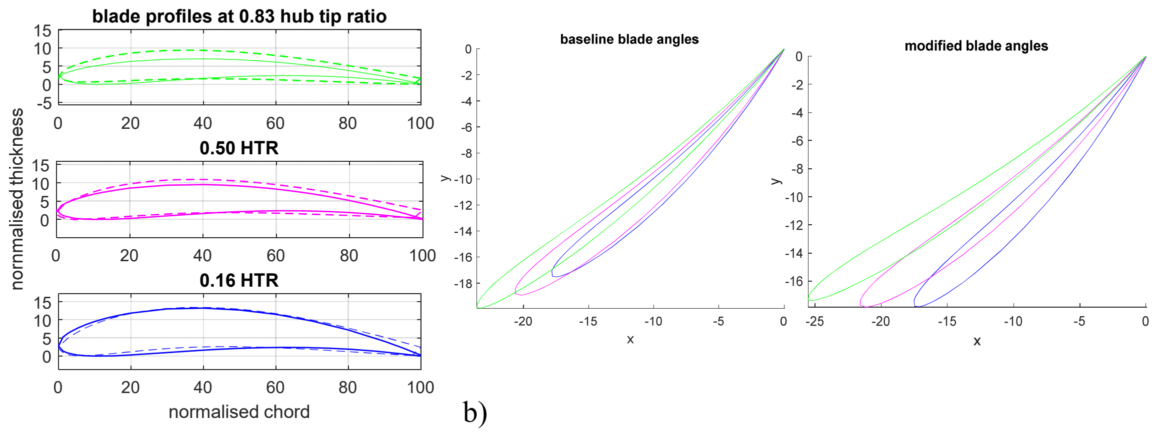

a) b)

Figure 11: a) Non-dimensionalised blade profiles for the baseline (dash line) and modified rotor (solid line) at each working radius; b) blade angles and chords for the baseline and modified blade.

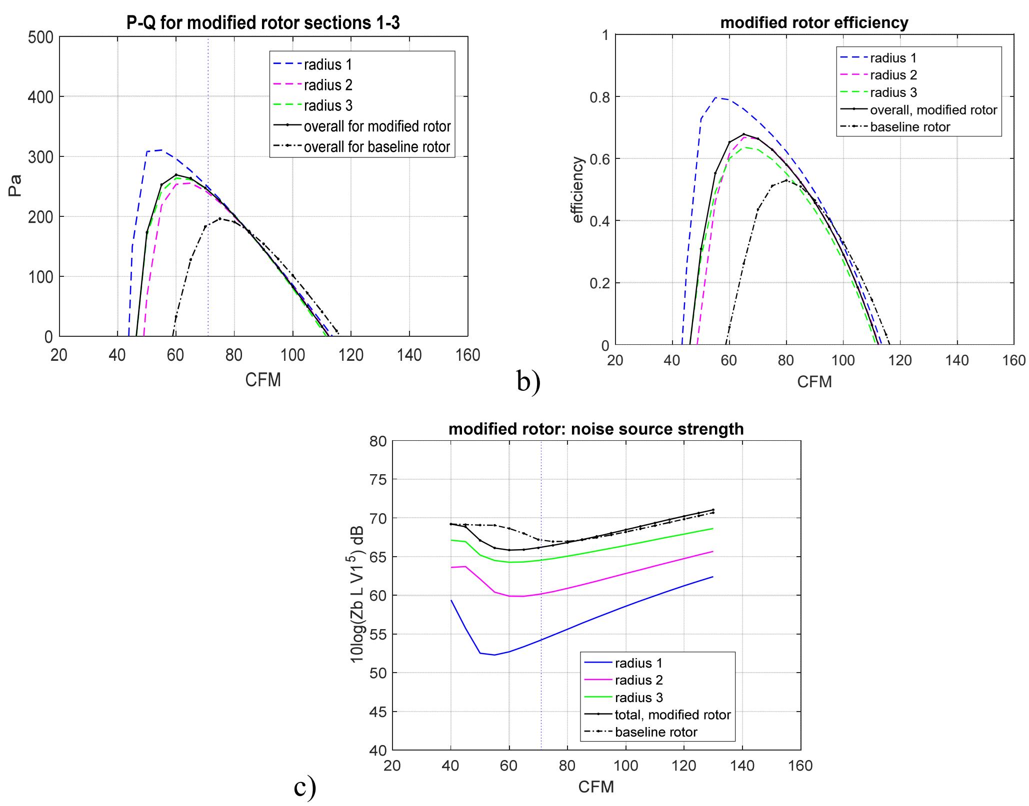

a) b) c)

Figure 12: Predicted performance, efficiency and noise source strength for the modified rotor.

6.2. Numerical model

Having developed the design using the 2-D model, it was then validated using the CFD analysis. Furthermore, the 3-D model was used to look at the effect of blade sweep, the details of the tip feature, the aerodynamic interactions between the rotor and stator, and the changes in turbulence intensity in the flow shed by the rotor.

Figure 13 shows the frontal view of the original rotor and three modified designs: with and without blade sweep, and with a winglet at the blade tip. Adding a winglet is generally considered beneficial for the noise [8], because of the positive effect on the tip vortex, even if it could be detrimental for the rotor aerodynamic performance. The size of the winglet was kept to a minimum, covering about 6% of the blade length compared with 15% for the winglet of the original rotor.

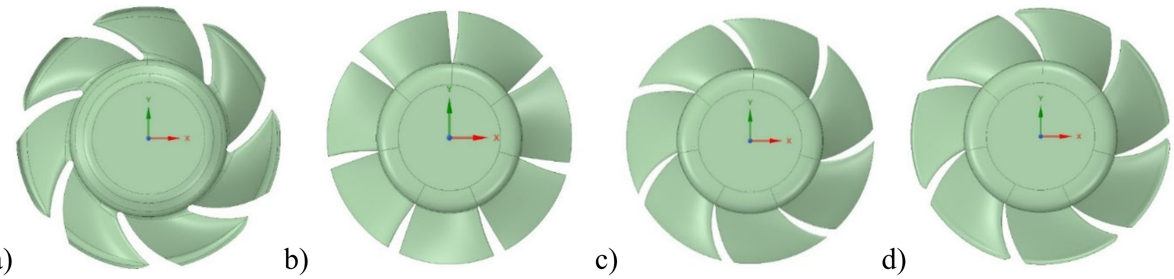

a) b) c) d)

Figure 13: Frontal view of the original rotor (a) and the modified rotor with different 3D features: b) without blade sweep; c) with blade sweep; d) with a winglet at the blade tip.

Simulations were carried out first for the rotor alone, and the results in Figure 14 show that:

- The 3D blade sweep has an important effect on rotor performance, maximizing the potential performance of the rotor and increasing the maximum efficiency by 10%.
- As predicted by the 2D method, there is a clear improvement of the new design over the original rotor performance, with both increased pressure and 10% improvement in efficiency.
- The rotor with tip winglet underperforms compared with the case without winglet, however the difference is less than 6% of maximum efficiency. This is counterbalanced by a benefit on turbulence, and further improves when the stator is included, see Figures 15 and 16.
- The turbulence kinetic energy downstream of the rotor is shown in Figure 15. Turbulence level at approximately 130 CFM is much lower for the modified rotor design, and tip turbulence is improved by including the winglet.

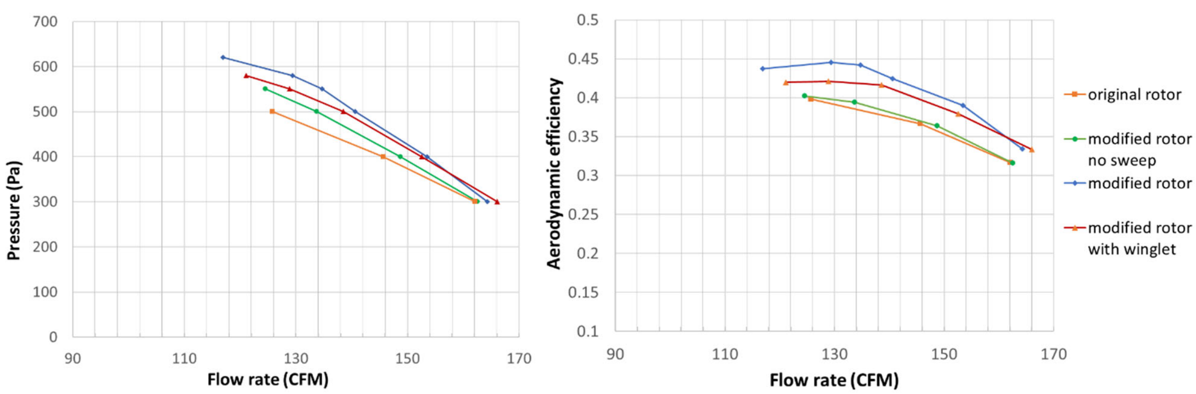

Figure 14: Predicted P-Q and efficiency curves for the modified designs compared with the original rotor, rotor alone.

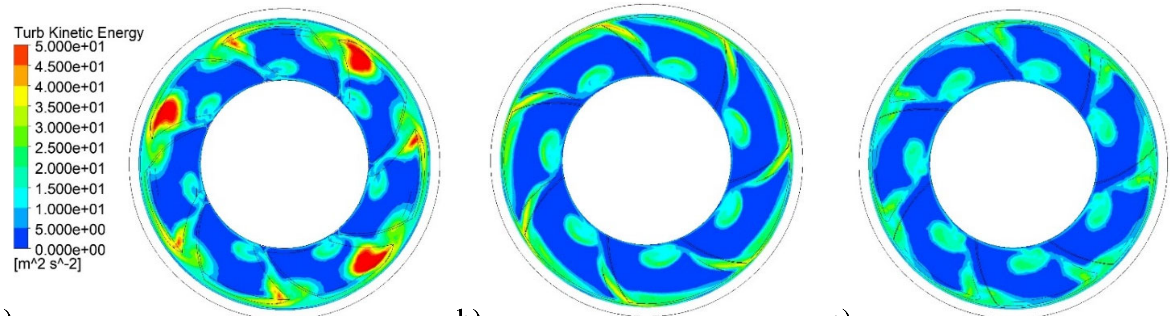

a) b) c)

Figure 15: Turbulence Kinetic Energy downstream of the rotor at approximately 130 CFM: a) original rotor; b) modified design without winglet; c) modified design with winglet.

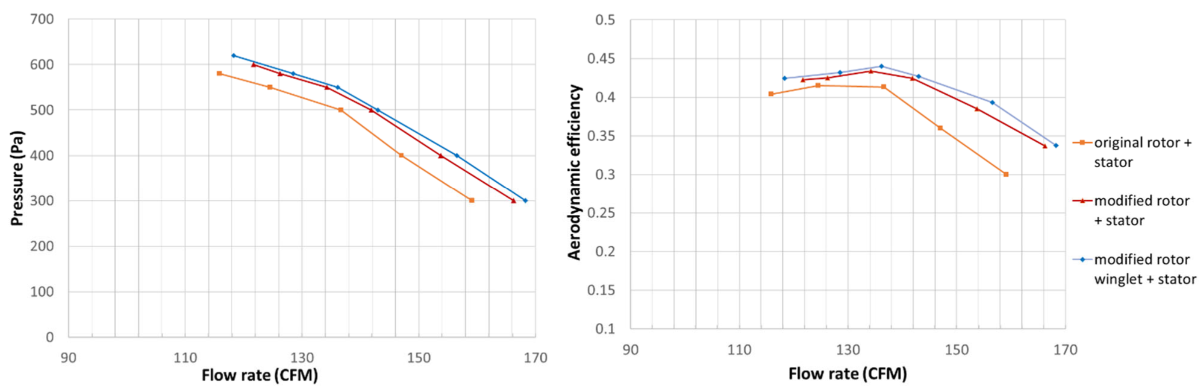

Figure 16: Predicted P-Q and efficiency curves for the new rotor designs compared with the original rotor, including the stator.

After comparing the rotor-alone designs, a stator was included in the simulation. Figure 16, confirms the improvement of the modified design over the original rotor. It is also interesting that the difference between the baseline and the tip winglet blade is greatly reduced, with the winglet blade now being more efficient. Considering Figure 17, the different trend in turbulence level is also confirmed. This could be the reason for the winglet blade performing better when turbulence from the rotor is impacting on the stator.

The latter effect is even more important when the noise is considered, and the development of a noise model based on the CFD data has been initiated by predicting noise from the stator blades, even if they are considered a secondary source for this fan and have been estimated to be at least 5dB lower than the rotor noise.

Following Blandeau [9] in the low Mach number approximation, the sound power radiated by a single flat plate can be correlated to the fluid and turbulence properties. Figure 18 shows how the relevant flow variables (mean velocity, turbulence length scale and mean square velocity fluctuation) are distributed along the radius in 9 sectors, corresponding to the 9 stator blades, on the interface between the rotor and stator, and comparing the original rotor (dashed lines) with the modified design with winglet (continuous lines). The assumption here is that each stator blade acts in isolation, and interactions between blades are neglected.

Figure 18 confirms that turbulence level is higher in the middle/tip blade area for the original rotor, while it is lower at the root. When the total sound pressure level radiated by the stator blades is evaluated using this approximation, the difference in turbulence levels translates into 2dB improvement, as shown in Figure 19.

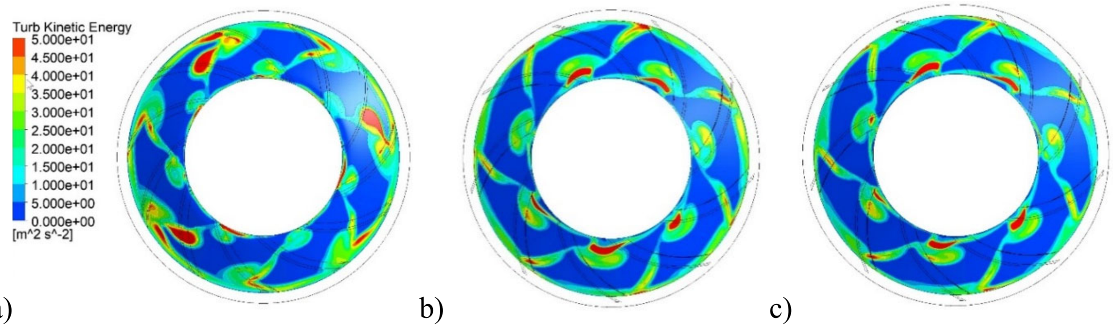

Figure 17: Turbulence Kinetic Energy on a plane between the rotor and stator at approximately 135 CFM: a) original rotor; b) modified design without winglet; b) modified design with winglet.

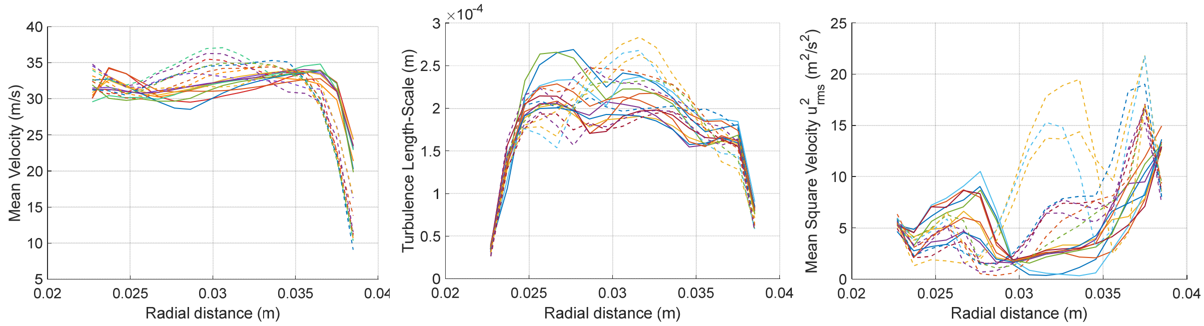

Figure 18: Variation of flow variables along the radius averaged on 9 sectors: a) Mean velocity; b) Turbulence length scale; c) Mean square velocity fluctuation. Continuous lines for modified rotor with winglet, dashed lines for original rotor.

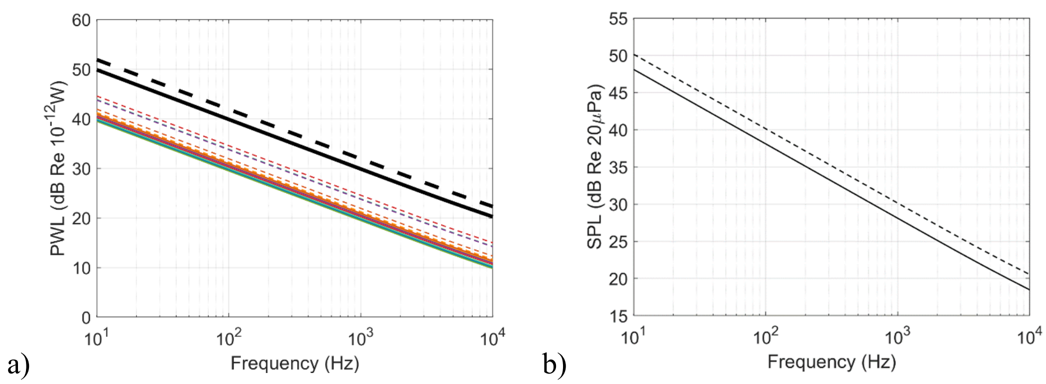

Figure 19: a) Sound Power Level (dB) vs frequency for each sector (color) and total (black). b) Sound pressure level (dB) considering a spherical spreading at 0.5 m from the fan.

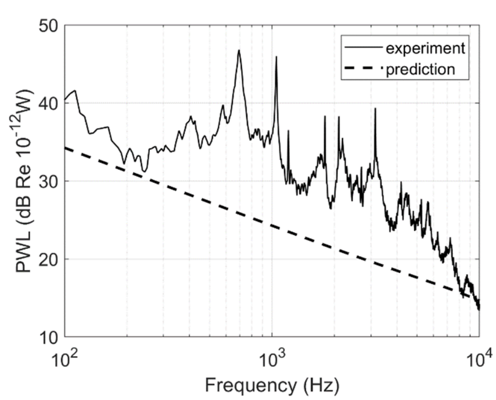

Figure 20: Comparison between experimental and predicted sound power level for the original rotor at 9000 RPM.

Using noise data for a single test point of the original rotor, with SPL integrated over a hemisphere to give sound power (PWL), Figure 20 shows a comparison between predicted and measured PWL. Considering that only the noise due to the turbulence impinging on the stator is predicted here, the overall trend and level appear to be good, although more validation and development of the method is required. In due course the method will also be extended to include the rotor trailing edge source.

7. CONCLUSIONS AND FURTHER PLANNED DEVELOPMENTS

The results of this study suggest that the proposed design methodology shows significant promise. The 2-D model was able to identify deficiencies in the design of the baseline fan, and suggest remedial modifications that the CFD model has predicted will significantly improve performance. Experimental validation of this aerodynamic result is under way, and it is also hoped to carry out noise testing in order to confirm any changes in noise source strength.

There is considerable scope for development of both the aerodynamic and noise modelling aspects:

- For the analytic aerodynamic model a key improvement would be to better utilize available aerofoil design tools for estimating lift and drag coefficients as a function of profile shape, Reynolds number and 3-D design factors such as blade sweep. Stator design can also be included.
- For the 2D noise prediction model, this can readily be extended to include all parameters in Equation 10 and to include a full model of the stator noise. There is also potential to take account of inflow turbulence to build a model of installed fan noise.
- Once a full model of the noise and performance has been implemented, this could be used to develop a design optimization tool to produce designs that fit a specific space envelope.
- It has also been shown how the CFD model can be developed into a noise prediction tool, and although this is still at an early stage of development, a trailing edge noise model can be included.

8. ACKNOWLEDGEMENT

The authors would like to thank Yu Sun, Chihfeng Hu and Huawei Technologies Co for permission to use experimental data and modelling results from our research collaboration. We also want to acknowledge the use of the HPC facility Iridis 4 at the University of Southampton for running all the CFD cases.

9. REFERENCES

1. ANSI/AMCA Standard 210, Laboratory method of testing fans for aerodynamic performance rating, *Air Movement and Control Association International*, Inc., 2000.
2. Bleier, F. P. Fan Handbook: selection, application and design, *McGraw Hill,* 1997.
3. Wallis, R. A. Axial flow fans and ducts, *J. Wiley*, 1983.
4. Eck, B. Fans: Design and operation of centrifugal, axial flow and cross flow fans. *Pergamon Press*, 1st English Edition, 1973.
5. Drela, M. XFOIL: An analysis and design system for low Reynolds number airfoils, Low Reynolds Number Aerodynamics, *Springer-Verlag*, 1989.
6. Abbott, I. H. & von Doenhoff, A. E. Theory of wing sections, including a summary of airfoil data. *Dover Publication,* N. Y., 1959.
7. Ffowcs-Williams J.E. and Hall L.H Aerodynamic sound generation by turbulent flow in the vicinity of a scattering half plane. *Journal of Fluid Mechanics 1970 Vol 40 part 4*
8. Bizjan, B., Milavec, M., Sirok, B. Trenc, K. & Hocevar, M. Energy dissipation in the blade tip region of an axial fan, *Journal of Sound and Vibration,* **382**, 63-72 (2016).
9. Blandeau, V. P., Joseph, P. F., Jenkins, G. & Powles, J. C. Comparison of sound power radiation from isolated airfoils and cascades in a turbulent flow. (ASA, Ed.) *The Journal of the Acoustical Society of America*, **129(6)**, 3521-3530 (2001).